Tensor monopoles and the negative magnetoresistance effect in optical lattices

Hai-Tao Ding,[1] Yan-Qing Zhu,[1,*] Zhi Li,[3] and Lubing Shao[1,†]

[1]*National Laboratory of Solid State Microstructures and School of Physics, Nanjing University, Nanjing 210093, China*

[2]*Guangdong Provincial Key Laboratory of Quantum Engineering and Quantum Materials, School of Physics and Telecommunication Engineering, South China Normal University, Guangzhou 510006, China*

[3]*Guangdong-Hong Kong Joint Laboratory of Quantum Matter, South China Normal University, Guangzhou 510006, China*

(Received 4 July 2020; revised 29 October 2020; accepted 12 November 2020; published 30 November 2020)

We propose that a kind of four-dimensional (4D) Hamiltonians, which host tensor monopoles related to the quantum metric tensor in even dimensions, can be simulated by ultracold atoms in optical lattices. The topological properties and bulk-boundary correspondence of tensor monopoles are investigated in detail. By fixing the momentum along one of the dimensions, it can be reduced to an effective three-dimensional model manifesting with a nontrivial chiral insulator phase. Using the semiclassical Boltzmann equation, we calculate the longitudinal resistance against the magnetic field B and find a negative relative magnetoresistance effect with approximately $-B^2$ dependence when a hyperplane cuts through the tensor monopoles in the parameter space. We also propose an experimental scheme to realize this 4D Hamiltonian by introducing an external cyclical parameter in a 3D optical lattice. Moreover, we show that the quantum metric tensor and Berry curvature can be detected by applying an external drive in the optical lattices.

DOI: 10.1103/PhysRevA.102.053325

I. INTRODUCTION

In 1931, Dirac introduced the concept of monopoles to explain the quantization of electron charge [1]. Since then, the development of gauge theory has shown that monopoles emerge in a natural way in all theories of grand unification. However, the existence of the monopole as an elementary particle has not been confirmed by any experiment to date. Monopoles in momentum space have attracted extensive studies in condensed matter physics and artificial quantum systems, such as Dirac monopoles in Weyl semimetals. The celebrated Nielsen-Ninomiya theorem states that Weyl points in the first Brilluoin zone must emerge and annihilate in pairs with opposite chirality, which provides a mechanism of anomaly cancellation in the field theorem framework [2]. Moreover, the negative magnetoresistance (MR) effect, in which longitudinal conductivity increases along with increasing magnetic field, has been reported in several experiments and can be interpreted as a result of the suppression of backscattering due to the chirality of the monopoles in Weyl semimetals [3–9]. Besides those monopoles in odd dimensions, recent research shows that another kind of monopoles can emerge in even dimensions, named "tensor monopoles," which are Abelian monopoles associated with the tensor (Kalb-Ramond) gauge field [10]. The topological charge of the tensor monopole is related to the so-called quantum metric tensor which measures the distance of two nearby states in the parameter space. Recently, by using controllable quantum systems, several experiments have been reported to directly measure the quantum metric tensor, which characterizes the geometry and topology of underlying quantum states in parameter space [11–14]. More recently, two experiments for realizing the tensor monopoles in four-dimensional (4D) parameter space have been reported in a superconducting circuit system[15] and the nitrogen-vacancy (NV) center in diamond [16], respectively.

The technology of ultracold atoms provides an excellent platform to study different topological systems of condensed matter and high-energy physics, because of its perfect cleanness and high controllability [17]. Recently, the 4D quantum Hall effect was also experimentally simulated by ultracold atoms, which opens up the research of high-dimensional physics in realistic systems [18,19]. It shows that an extra dimension can be engineered by a set of internal atomic levels as a synthetic lattice dimension [20,21]. The 4D Hamiltonian can also be realized in a 3D optical lattice with a cyclical parameter playing the role of the pseudomomentum of the fourth dimension [22–27]. In order to measure the Berry phase of topological systems in cold atoms, many experimental approaches have been proposed and conducted, including state tomography [28,29], interferometry [30], and atomic transport [31]. A recent development on how to measure the quantum metric tensor and Berry curvature by shaking the optical lattice has promoted research into tensor monopoles with cold atoms [12,32].

In this paper, we propose two minimal Hamiltonians in 4D which host tensor monopoles [10,33–36], and then study their topological properties. Tensor monopoles in these two systems can be considered as one conductance band, one valence band. and one flat band touching at the common points. and the topological properties of the tensor monopoles can be controlled by a tunable parameter. After fixing the momentum

*dg1722056@smail.nju.edu.cn

†lbshao@nju.edu.cn

of the fourth dimension in the parameter space, we obtain a 3D model. Rich phase diagrams can be derived from this 3D model, including a trivial phase and a chiral insulator phase. In addition, we calculate the MR with the semiclassical Boltzmann equation. When a hyperplane cuts through the tensor monopoles, the relative MR approximately proportional to $-B^2$ signifies the negative MR effect, where B is the magnetic field. We also propose an experimentally feasible scheme to implement our model with three-component ultracold atoms in a 3D optical lattice with an external parameter varying from $-\pi$ to π which can be treated as the fourth dimension. Moreover, we provide an experimental method to measure the quantum metric tensor and Berry curvature.

The paper is organized as follows. In Sec. II, we introduce the models for realizing tensor monopoles and review the definition of the quantum metric tensor with topological charge. In Sec. III, we give the tight-binding Hamiltonians and investigate the bulk-boundary correspondence. In Sec. IV, the MR effect is calculated for our tensor monopole models, using the semiclassical Boltzmann equation. In Sec. V, an experimental scheme to realize the 4D model is established with a proposal for measuring the quantum metric tensor and Berry curvature. Finally, a brief conclusion is provided in Sec. VI.

II. TENSOR MONOPOLES IN 4D FLAT SPACE

Following Ref. [37], the tensor monopole in momentum space can be hosted by a generalization of the 4D multi-Weyl Hamiltonian as

$$H_n = \tfrac{1}{2}(k_-^n\lambda_+ + k_+^n\lambda_-) + \alpha_z k_z\lambda_6 + \alpha_w k_w\lambda_7^*, \tag{1}$$

where $\mathbf{k} = (k_x, k_y, k_z, k_w)$ is the 4D momentum. The λ_i ($i = 1, 2, 6, 7$) are Gell-Mann matrices [38], which are representations of the infinitesimal generators of SU(3). Here we set $k_\pm = k_x \pm \mathrm{i}k_y$ and $\lambda_\pm = \alpha_x\lambda_1 \pm i\alpha_y\lambda_2$, $\alpha_j = \pm 1$ ($j = x, y, z, w$). The Hamiltonian breaks time reversal symmetry, but keeps chiral symmetry due to the anticommutative relation $\{U, H_n\} = 0$ with $U = \mathrm{diag}(1, -1, 1)$. Energy spectra are obtained as

$$E_\pm = \pm\sqrt{\left(k_x^2 + k_y^2\right)^n + k_z^2 + k_w^2}, \quad E_0 = 0. \tag{2}$$

The related eigenstates are denoted by $|u_\pm\rangle$, $|u_0\rangle$. The tensor monopole exists at $\mathbf{k} = (0, 0, 0, 0)$, where the three bands touch commonly.

Recall that the Dirac monopoles and non-Abelian Yang monopoles are defined in 3D and 5D parameter spaces, respectively. They are all described by vector Berry connections, i.e., the vector gauge field. But for tensor monopoles defined in 4D parameter space, they are captured by the tensor Berry connection. The associated gauge field is an Abelian antisymmetric tensor field $B_{\mu\nu}$ called the Kalb-Ramond field, which is defined as

$$B_{\mu\nu} = \phi F_{\mu\nu},$$
$$\phi = -\frac{i}{2}\ln\prod_{\aleph=1}^{3} u_-^{\aleph}, \tag{3}$$

Here ϕ is a pseudoscalar gauge field, $F_{\mu\nu} = \partial_\mu A_\nu - \partial_\nu A_\mu$ is Berry curvature($\partial_\mu \equiv \partial_{k_\mu}$) with the associated Berry connection $A_\mu = \langle u_-|i\partial_\mu|u_-\rangle$, and $u_-^{\aleph}$ denotes the components of the lowest band $|u_-\rangle$ [39]. The related 3-form curvature is $\mathcal{H} = dB$, whose components are given by

$$\mathcal{H}_{\mu\nu\lambda} = \partial_\mu B_{\nu\lambda} + \partial_\nu B_{\lambda\mu} + \partial_\lambda B_{\mu\nu}. \tag{4}$$

It is gauge invariant and antisymmetric. For the Hamiltonian in Eq. (1), the corresponding 3-form curvature is

$$\mathcal{H}_{\mu\nu\lambda} = \mathrm{sgn}(\alpha_x\alpha_y\alpha_z\alpha_w)\epsilon_{\mu\nu\lambda\gamma}\frac{nk_\gamma}{\left(k_x^2 + k_y^2 + k_z^2 + k_w^2\right)^2}. \tag{5}$$

A topological charge associated with this curvature $\mathcal{H}_{\mu\nu\lambda}$ can be defined by surrounding the tensor monopole with a sphere S^3,

$$Q_n = \frac{1}{2\pi^2}\int_{S^3} dk^\mu \wedge dk^\nu \wedge dk^\lambda \mathcal{H}_{\mu\nu\lambda}. \tag{6}$$

This is a topological invariant known as the Dixmier-Douady (DD) invariant, which is related to the (first) Dixmier-Douady class of U(1) "bundle gerbes" [40–43].

Directly measuring the tensor Berry curvature in experiments actually is difficult. Fortunately, we can find a direct relation between the components of 3-form curvature and the quantum metric (or Fubini-Study metric) [10],

$$\mathcal{H}_{\mu\nu\lambda} = \mathrm{sgn}(\alpha_x\alpha_y\alpha_z\alpha_w)\epsilon_{\mu\nu\lambda}(4\sqrt{\det g_{\bar{\mu}\bar{\nu}}}), \tag{7}$$

where $g_{\bar{\mu}\bar{\nu}}$ is the 3×3 quantum-metric tensor defined in the proper 3D subspace. Physically, if the Hamiltonian of a system is parametrized as $H \equiv H(\vec{\lambda})$, the quantum metric tensor measures the (infinitesimal) distance between two nearby quantum states, $ds^2 = 1 - |\langle\psi_\lambda|\psi_{\lambda+d\lambda}\rangle|^2$, in $\vec{\lambda}$ space [44] as

$$ds^2 = \sum_{\mu\nu} g_{\mu\nu} d\lambda_\mu d\lambda_\nu, \tag{8}$$

in which the metric tensor can be explicitly written as

$$g_{\mu\nu} = \mathrm{Re}\left(\left\langle\frac{\partial\psi}{\partial\lambda_\mu}\middle|\frac{\partial\psi}{\partial\lambda_\nu}\right\rangle - \left\langle\frac{\partial\psi}{\partial\lambda_\mu}\middle|\psi\right\rangle\langle\psi|\frac{\partial\psi}{\partial\lambda_\nu}\right\rangle\right). \tag{9}$$

Obviously, the metric is positive and satisfies $g_{\mu\nu} = g_{\nu\mu}$. As a consequence, Eq. (7) provides a feasible method to detect the 3-form curvature through quantum metric tensor measurement, which will be discussed in Sec. V.

In other words, one can calculate the DD invariant through the quantum metric tensor. To be more clear, we show some derivations of the DD invariant by calculating the quantum metric below. For simplify, we can parametrize the momentum space $\mathbf{k} = (k_x, k_y, k_z, k_w)$ in Eq. (1) with the hyperspherical coordinates $(k, \theta_1, \theta_2, \varphi)$ as

$$\begin{aligned} k_x &= (k\sin\theta_1\sin\theta_2)^{\frac{1}{n}}\cos\varphi, \\ k_y &= (k\sin\theta_1\sin\theta_2)^{\frac{1}{n}}\sin\varphi, \\ k_z &= k\sin\theta_1\cos\theta_2, \\ k_w &= k\cos\theta_1, \end{aligned} \tag{10}$$

where $k = \sqrt{\left(k_x^2 + k_y^2\right)^n + k_z^2 + k_w^2}$ is the radius of the 3-hypersphere encircling the monopole in momentum space.

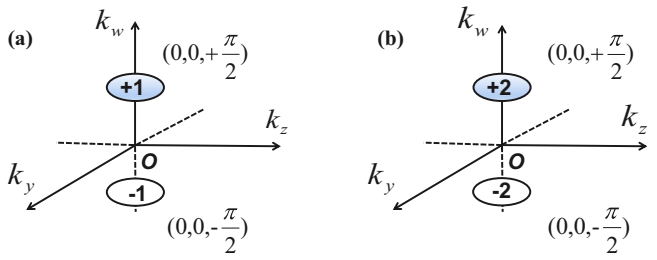

FIG. 1. (a) and (b) are the monopoles of $\mathcal{H}_1$ and $\mathcal{H}_2$ for $h = 3$. We plot the monopoles in k_y-k_z-k_w parameter space and define $k_x = 0$. The ellipses stand for monopoles and the numbers mean their topological charges.

If the lowest energy band $\varepsilon_{\mathbf{k}} = -k$ is filled, the topological charge of the tensor monopole can be defined as

$$Q_n = \frac{1}{2\pi^2}\int_0^{\pi} d\theta_1 \int_0^{\pi} d\theta_2 \int_0^{2\pi} d\varphi \mathcal{H}_{\theta_1\theta_2\varphi}, \tag{11}$$

where $\mathcal{H}_{\theta_1\theta_2\varphi} = 4\,\mathrm{sgn}(\alpha_x\alpha_y\alpha_z\alpha_w)\sqrt{\det g}$. By considering the hypersphere surrounding the monopole, we derive $\det g = \frac{1}{16}n^2 \sin^4\theta_1 \sin^2\theta_2$ and the topological charge is obtained as

$$Q_n = n\,\mathrm{sgn}(\alpha_x\alpha_y\alpha_z\alpha_w). \tag{12}$$

We consider two special cases of the Hamiltonians in Eq. (1) as

$$H_1 = k_x\lambda_1 + k_y\lambda_2 + k_z\lambda_6 + k_w\lambda_7^*, \tag{13}$$

for $n = 1$, and

$$H_2 = \left(k_x^2 - k_y^2\right)\lambda_1 + 2k_xk_y\lambda_2 + k_z\lambda_6 + k_w\lambda_7^*, \tag{14}$$

for $n = 2$. In both cases, the three energy bands all cross at $\mathbf{k} = (0, 0, 0, 0)$, which hosts tensor monopoles with the topological charges being $Q_1 = 1$ and $Q_2 = 2$, respectively.

III. THE MINIMAL MODELS IN MOMENTUM SPACE

Now we construct the Hamiltonians in Eq. (13) and (14) with the tight-binding models in the momentum space as

$$\mathcal{H}_n = d_{n,x}\lambda_1 + d_{n,y}\lambda_2 + d_{n,z}\lambda_6 + d_{n,w}\lambda_7^*, \tag{15}$$

with $n = 1, 2$.

For $n = 1$, the explicit forms of d's are

$$\begin{aligned} d_{1,x} &= 2t\sin k_x, \\ d_{1,y} &= 2t\sin k_y, \\ d_{1,z} &= 2t\sin k_z, \\ d_{1,w} &= 2t(h - \cos k_x - \cos k_y - \cos k_z - \cos k_w), \end{aligned} \tag{16}$$

where we have set the lattice constant $a = 1$. Here, t is the hopping energy and h is a tunable parameter. The corresponding spectrum is given by $\{0, \pm\sqrt{d_{1,x}^2 + d_{1,y}^2 + d_{1,z}^2 + d_{1,w}^2}\}$. When $h = 3$, there exist a pair of triple-degenerate Dirac-like points at $\mathbf{K}_{\pm} = (0, 0, 0, \pm\pi/2)$, which are tensor monopoles with topological charges ±1, as shown in Fig. 1(a) with $k_x = 0$. The $k \cdot p$ Hamiltonian near the two nodes with $\mathbf{q} = \mathbf{k} - \mathbf{K}_{\pm}$ yields the low-energy effective Hamiltonian as Eq. (13).

Similarly, for $n = 2$, the d's can be written as

$$\begin{aligned} d_{2,x} &= 2t(\sin^2 k_x - \sin^2 k_y), \\ d_{2,y} &= 4t\sin k_x \sin k_y, \\ d_{2,z} &= 2t\sin k_z, \\ d_{2,w} &= 2t(h - \cos k_x - \cos k_y - \cos k_z - \cos k_w), \end{aligned} \tag{17}$$

by which the energy dispersion is obtained as $\{0, \pm\sqrt{d_{2,x}^2 + d_{2,y}^2 + d_{2,z}^2 + d_{2,w}^2}\}$. For $h = 3$, there are also a pair of tensor monopoles at $\mathbf{K}_{\pm} = (0, 0, 0, \pm\pi/2)$ with topological charges ±2 as shown in Fig. 1(b) with $k_x = 0$. The low-energy effective Hamiltonian near the two nodes is obtained as Eq. (14).

For both cases of $n = 1$ and $n = 2$, the combination and division of tensor monopoles inside the first Brillouin zone (FBZ) are controlled by the parameter h. For $h = 0$, there are six trivial monopoles located at $(\pi, \pi, 0, 0)$, $(\pi, 0, \pi, 0)$, $(\pi, 0, 0, \pi)$, $(0, \pi, \pi, 0)$, $(0, \pi, 0, \pi)$, and $(0, 0, \pi, \pi)$. Increasing h, the six monopoles begin to move in the FBZ. When $h = 1$, the six degenerate points move to $(0, 0, \pi, \pm\pi/2)$, $(0, \pi, 0, \pm\pi/2)$, $(\pi, 0, 0, \pm\pi/2)$, including three of them with positive topological charge and three others with negative topological charge as a result of the generalized Nielsen-Ninomiya theorem [2]. When continuously increasing h to $h = 2$, there are four monopoles left at $(\pi, 0, 0, 0)$, $(0, \pi, 0, 0)$, $(0, 0, \pi, 0)$, $(0, 0, 0, \pi)$, which are also trivial. For $h = 3$, only two monopoles are left at $(0, 0, 0, \pm\pi/2)$. For $h = 4$, the two monopoles move toward $(0, 0, 0, 0)$ and combine to open a gap. Finally, it becomes a topologically trivial insulator for $h > 4$.

By taking a slice of these two 4D models, i.e., fixing $k_w = 0$, 3D models can be derived from the 4D systems. The topological nature of the 3D system is captured by the DD invariant. This invariant is equivalent to the winding number, which characterizes 3D topological insulators in class AIII [45–47]:

$$\begin{aligned} \Gamma_n &= \frac{1}{12\pi^2}\int_{BZ} d^3k\,\epsilon^{\alpha\beta\gamma\rho}\epsilon^{\mu\nu\tau}\frac{1}{E_+^4}d_\alpha\partial_\mu d_\beta\partial_\nu d_\gamma\partial_\tau d_\rho \\ &= Q_n, \end{aligned} \tag{18}$$

where $E_+(k) = \sqrt{d_{n,x}^2 + d_{n,y}^2 + d_{n,z}^2 + d_{n,w}^2}$, and the indexes of the Levi-Civita symbol with $\alpha, \beta, \gamma, \rho$ and μ, ν, τ represent $\{x, y, z, w\}$ and $\{k_x, k_y, k_z\}$, respectively.

Another equivalent way to characterize the topology of the 3D models is the Chern-Simons invariant (CSI), which takes the form

$$\mathrm{CS} = \frac{1}{4\pi}\int_{\mathrm{BZ}} d\mathbf{k}\,\epsilon^{\mu\nu\tau}A_\mu(\mathbf{k})\partial_\nu A_\tau(\mathbf{k}), \tag{19}$$

where $A_\mu(\mathbf{k}) = \langle u(\mathbf{k})|i\partial_\mu|u(\mathbf{k})\rangle$ $(\mu = x, y, z)$ [45,48]. We plot the CSI against h in Fig. 2(a) with $n = 1$ and in 2(b) with $n = 2$ for the three energy bands at $k_w = 0$. The relation of its value between different bands is

$$\mathrm{CS}_n(+) = \mathrm{CS}_n(-) = \tfrac{1}{4}\mathrm{CS}_n(0). \tag{20}$$

As indicated in Fig. 2, the topological phase transitions occur at $h = 0, \pm2, 4$, when the three bands touch at the hyperplane of $k_w = 0$. For $h \in (-2, 4)$, CS_n is nonzero; they are topologically nontrivial phases here. A detailed calculation shows that

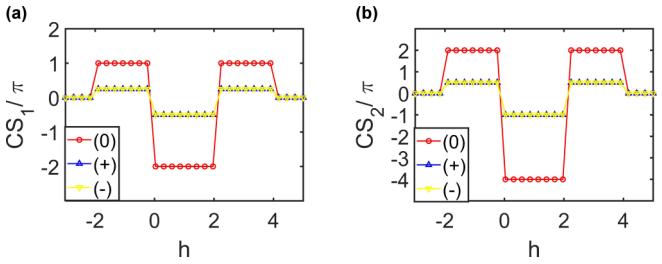

FIG. 2. (a) and (b) represent the Chern-Simons terms of $\mathcal{H}_1$ and $\mathcal{H}_2$ respectively. (+) stands for the positive energy band, (0) and (−) represent the flat and negative energy bands respectively. Here we set $t = 1$.

the relation between winding number and the Chern-Simons term is

$$\frac{\pi}{4}\Gamma_n = \mathrm{CS}_n(-). \tag{21}$$

When $h = 5$, according to Fig. 2, the 3D system is trivial and no surface state exists, which is confirmed by the numerical calculations shown in Fig. 3(c) and 3(d). The energy spectrum and surface states with an open boundary along the $\hat{z}$ direction are shown in Fig. 3. As discussed before, for $h = 3$, two tensor monopoles are located at $(0, 0, 0, \pm\pi/2)$ and the spectrum is gapped and topologically nontrivial for $k_w \in (-\pi/2, \pi/2)$. They are chiral insulator phases. Therefore, there are surface states of Dirac cones for those sliced 3D systems until the slicing hyperplane hits the tensor monopoles. Namely, the surface Dirac cone survives when $-\pi/2 < k_w < \pi/2$. The spectra with $k_w = 0$ are shown in Figs. 3(a) and 3(b) for $n = 1$ and $n = 2$, respectively. When we take the slicing hyperplane perpendicular to the $\hat{x}$ axis, the sets of those Dirac points constitute the Fermi arcs connecting two tensor monopoles for $n = 1$ and $n = 2$, which are shown in Figs. 4(a) and 4(c), respectively. Figs. 4(b) and 4(d) show the density distribution of surface states. By using the method in

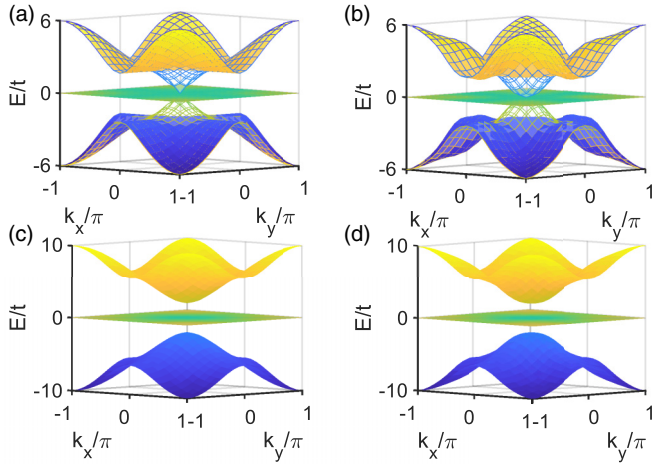

FIG. 3. The bulk state (surface plot) and surface state (mesh plot), for $k_w = 0$. (a) is the case of $\mathcal{H}_1$, $h = 3$. (b) is $\mathcal{H}_2$, $h = 3$. They are chiral topological insulator phases; the surface state connects three gapped bands. (c) and (d) show the bulk states of $\mathcal{H}_1$, $h = 5$ and $\mathcal{H}_2$, $h = 5$. They are trivial insulators.

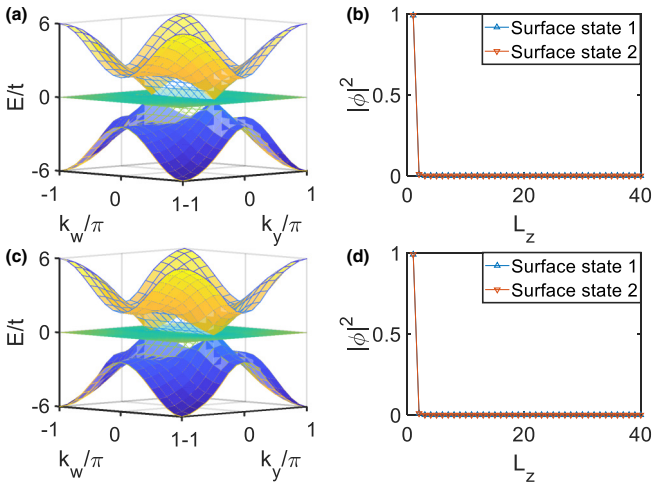

FIG. 4. (a) and (c) are the bulk state (surface plot) and surface state (mesh plot) of $\mathcal{H}_1$ and $\mathcal{H}_2$ respectively. (b) and (d) are the density distributions of the wave functions of surface states for $\mathcal{H}_1$ and $\mathcal{H}_2$ respectively. Here $k_x = 0$, $k_y = k_w = 0.1\pi$.

Ref [45], for $k_w \in (-\pi/2, \pi/2)$, the low-energy spectra of surface states around $(k_x, k_y, k_z) = (0, 0, 0)$ are $\pm v\sqrt{k_x^2 + k_y^2}$ and $\pm v(k_x^2 + k_y^2)$ for $n = 1$ and $n = 2$, respectively. Here $v = 2t$ is the effective Fermi velocity. A detailed derivation of these spectra can be found in the Appendix.

IV. TRANSPORT PROPERTY

The negative magnetoresistance effect has already been extensively discussed in topological semimetals. This fantastic transport phenomena is widely believed to be caused by a chiral anomaly, which is the violation of the conservation of chiral current [5]. In some topological insulators, the same effect also emerges, although the chiral anomaly is not well defined in these systems [49,50]. By using the semiclassical equation, we can calculate MR.

In the semiclassical limit, the electronic transport can be described by the equations of motion

$$\begin{aligned}
\dot{\mathbf{r}} &= \frac{1}{\hbar}\nabla_{\mathbf{k}}\tilde{\varepsilon}_{\mathbf{k}} - \dot{\mathbf{k}} \times \mathbf{\Omega}_{\mathbf{k}}, \\
\dot{\mathbf{k}} &= -\frac{e}{\hbar}(\mathbf{E} + \dot{\mathbf{r}} \times \mathbf{B}), \\
\tilde{\varepsilon}_{\mathbf{k}} &= \varepsilon_{\mathbf{k}} - \mathbf{M} \cdot \mathbf{B}, \\
\mathbf{M} &= -\frac{e}{2h}\,\mathrm{Im}\left\langle \frac{\partial u}{\partial \mathbf{k}} \middle| \left(\mathcal{E}_0 - \hat{H}_0(\mathbf{k})\right) \middle| \frac{\partial u}{\partial \mathbf{k}} \right\rangle,
\end{aligned} \tag{22}$$

which describe the dynamics of the wave packet [51–53]. Here, $\mathbf{r}$ is the position of the wave packet in real space and $\mathbf{k}$ corresponds to the wave vector. $\mathbf{\Omega}_{\mathbf{k}}$ is the Berry curvature, $\varepsilon_{\mathbf{k}}$ is the energy dispersion of the valence band, and $\mathbf{M}$ is the orbital magnetic moment of the wave packet which is analogous to the magnetic moment of an electron's motion around the nucleus [54].

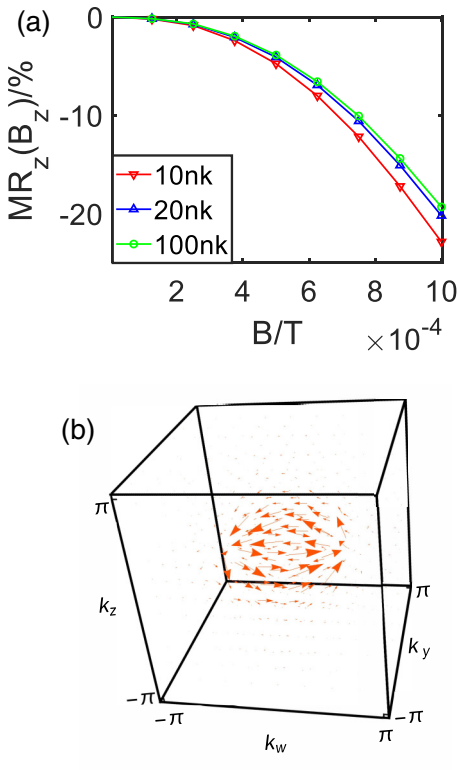

FIG. 5. (a) The relative MR with $n = 1$ and $h = 3$, $k_x = 0$. The magnetic field is applied along $\hat{z}$ direction, the lattice spacing $a =$ 382 nm, $t/\hbar = 2\pi \times 40$ Hz, and $E_F = -0.1t$. (b) The vector distribution of the Berry curvature $\mathbf{\Omega_k}$ for $\mathcal{H}_1$ with $k_x = 0$.

Using the semiclassical Boltzmann equation, the longitudinal conductivity can be calculated by

$$\sigma^{\mu\mu} = \int \frac{d^3\mathbf{k}}{(2\pi)^3}\frac{e^2\tau}{D_\mathbf{k}}\left(\tilde{v}^\mu_\mathbf{k} + \frac{e}{\hbar}B^\mu \tilde{v}^\nu_\mathbf{k}\Omega^\nu_\mathbf{k}\right)^2\left(-\frac{\partial \tilde{f}_0}{\partial \tilde{\varepsilon}}\right),$$
$$D_\mathbf{k} = 1 + \frac{e}{\hbar}\mathbf{B}\cdot\mathbf{\Omega_k}, \tag{23}$$

where $\tilde{f}_0$ is the equilibrium Fermi distribution and τ is the lifetime of the quasiparticle in the semiclassical limit [50,55]. $\tilde{v}^\nu_\mathbf{k}$ and $\Omega^\nu_\mathbf{k}$ are the components of velocity and Berry curvature. In Fig. 5, for $n = 1$, $k_x = 0$, and $h = 3$, we plot the relative MR of the longitudinal resistance against the magnetic field B_z, which is defined as [50].

$$MR_z(B_z) = \frac{1/\sigma_{zz}(B_z) - 1/\sigma_{zz}(0)}{1/\sigma_{zz}(0)}, \tag{24}$$

and the results are plotted in Fig. 5(a); there is a typical $-B^2$ dependence of the MR, which signifies the negative MR effect along $\hat{z}$. The distribution of Berry curvature in the momentum space is plotted in Fig. 5(b), by which we find that the conventional topological charges for both Dirac points vanish. However, the negative MR can still be realized. Intuitively, it is because the coefficient of B^2 in Eq. (23) is always positive, regardless of whether or not the integral of $\mathbf{\Omega_k}$ on the sphere enclosing the Dirac point in 3D is zero. The typical experimental parameters of ultracold atoms in the optical lattice have been used in our calculation, while the magnetic field can be realized by an artificial gauge field for the experimental setup. Since the flat zero-energy band does not contribute to the conductance because of the vanishing velocity of the wave packet, we do not take the flat band into consideration.

V. IMPLEMENTATION SCHEME

A. Realization with optical lattices

In this subsection, we propose a scheme to realize the 4D Hamiltonian in Eq. (15) for $n = 1$ using ultracold atoms [7,56–58]. The simulation of this 4D system is achieved by parametrizing the momentum along $\hat{w}$ on the 3D optical lattice. For $n = 1$, we can use noninteracting fermionic atoms in a cubic optical lattice and choose three atomic internal states in the ground state manifold to encode the three spin states $|s\rangle$ ($s = \uparrow, 0, \downarrow$), where the cubic lattice can be formed with three orthogonal sets of counterpropagating laser beams with the same wave vector magnitude and orthogonal polarizations. The tight-binding Hamiltonian of this cold atom system with spin-dependent hopping is written as

$$\hat{H} = t\sum_\mathbf{r}[\hat{H}_\mathbf{rx} + \hat{H}_\mathbf{ry} + \hat{H}_\mathbf{rz} + \hat{H}']$$
$$\hat{H}_\mathbf{rx} = -i\hat{a}^+_{\mathbf{r}-\mathbf{x},0}(\hat{a}_{\mathbf{r},\uparrow} + \hat{a}_{\mathbf{r},\downarrow}) + i\hat{a}^+_{\mathbf{r}+\mathbf{x},0}(\hat{a}_{\mathbf{r},\uparrow} - \hat{a}_{\mathbf{r},\downarrow}) + \text{H.c.},$$
$$\hat{H}_\mathbf{ry} = \hat{a}^+_{\mathbf{r}-\mathbf{y},0}(\hat{a}_{\mathbf{r},\uparrow} - i\hat{a}_{\mathbf{r},\downarrow}) - \hat{a}^+_{\mathbf{r}+\mathbf{y},0}(\hat{a}_{\mathbf{r},\uparrow} + i\hat{a}_{\mathbf{r},\downarrow}) + \text{H.c.},$$
$$\hat{H}_\mathbf{rz} = -2i\hat{a}^+_{\mathbf{r}-\mathbf{z},0}\hat{a}_{\mathbf{r},\downarrow} + \text{H.c.},$$
$$\hat{H}' = 2i\gamma\hat{a}^+_{\mathbf{r},0}\hat{a}_{\mathbf{r},\downarrow} + \text{H.c.}, \tag{25}$$

where $\hat{H}_\mathbf{rx}$, $\hat{H}_\mathbf{ry}$, and $\hat{H}_\mathbf{rz}$ represent the hoppings along the x, y, and z axes, respectively, with the tunneling amplitude t and on-site flipping amplitude γ. $\hat{a}_{\mathbf{r},s}$ and $\hat{a}^+_{\mathbf{r},s}$ stand for the annihilation and creation operators on lattice site $\mathbf{r}$ for the spin state $|s\rangle$. In the tight-binding model, the spin-dependent atomic hopping between two nearest neighborhood sites can be realized by Raman coupling between their three spin states [59]. Here we define the on-site modulated parameter $\gamma = h - \cos\theta$; h is a constant and θ is a cyclical parameter that varies from $\theta = -\pi$ to $\theta = \pi$.

The generalized 3D tight-binding model on a simple cubic lattice Hamiltonian is

$$\hat{H} = \sum_{\tilde{\mathbf{k}},ss'}\hat{a}^+_{\tilde{\mathbf{k}},s}[\mathcal{H}_1(\tilde{\mathbf{k}},\theta)]_{ss'}\hat{a}_{\tilde{\mathbf{k}},s'}, \tag{26}$$

where $\tilde{\mathbf{k}} = (k_x, k_y, k_z)$. By treating the parameter θ as the pseudomomentum k_w, $\mathcal{H}_1(\mathbf{k})$ is the Bloch Hamiltonian as in Eq. (15) in a 4D parameter space $\mathbf{k} = (\tilde{\mathbf{k}}, \theta)$.

B. Detecting the quantum metric tensor and Berry curvature

We now turn to address an experimental method to detect the tensor monopole and measure negative magnetoresistance in our system, which is related to the measure of the quantum metric and Berry curvature in an optical lattice. The quantum metric tensor is the real part of the quantum geometric tensor, whose imaginary part is just the Berry curvature [60] and has been directly measured in some engineered systems [28–31,61,62]. In our paper, the basic experimental procedure is preparing the system in a given Bloch state and introducing an external drive by shaking the lattice [32,63–70]. Then the

quantum metric and Berry curvature can be measured by establishing their relationship with integrated excitation rate, which is a measurable quantity in experiments [12,32,71–75].

In order to measure the quantum metric tensor related to Eq. (15) with $n = 1$, the system is first prepared in the state of $e^{i\mathbf{k}^0\cdot\mathbf{r}}|u_-(\mathbf{k}^0)\rangle$. Shaking the lattice along the x direction results in a circular time-periodic perturbation given by

$$\hat{H}_{\hat{x}}(t) = \mathcal{H}_1 + 2E\hat{x}\cos(\omega t), \tag{27}$$

where E is drive amplitude and ω is the frequency of the shaking driving interband transitions [12,32]. After introducing this external drive, the excitation rate is given by

$$\Gamma_{\hat{x}}(\omega) = \sum_{n=0,+} |\langle u_n(\mathbf{k})|e^{-i\mathbf{k}\cdot\mathbf{r}}\hat{x}e^{i\mathbf{k}^0\cdot\mathbf{r}}|u_-(\mathbf{k}^0)\rangle|^2 \frac{2\pi E^2}{\hbar}\delta(\hbar\omega'), \tag{28}$$

which represents the probability of observing the system in other eigenstates per unit of time. Here $\hbar\omega' = E_n - E_- - \hbar\omega$. By integrating the rate over ω, we obtain

$$\Gamma^{\text{int}}_{\hat{x}} = \frac{2\pi E^2}{\hbar^2}\sum_{n=0,+} |\langle u_n(\mathbf{k}^0) \mid \partial_{k_x} u_-(\mathbf{k}^0)\rangle|^2. \tag{29}$$

The relation between the integrated excitation rate and the quantum metric tensor is now given by

$$\Gamma^{\text{int}}_{\hat{x}} = \int \Gamma_{\hat{x}}(w)d\omega = \frac{2\pi E^2}{\hbar^2} g_{xx}(\mathbf{k}^0), \tag{30}$$

where the diagonal component of quantum metric tensor $g_{xx} = \sum_{n=0,+} |\langle u_n|\partial_{k_x} u_-\rangle|^2$. The relation in Eq. (30) provides an experimentally feasible approach to measure the quantum metric tensor. In concrete practice, one can change the frequency to get the integrated excitation rate as [32,67,76]

$$\Gamma^{\text{int}}_{\hat{x}} = \sum_i \Gamma_{\hat{x}}(\omega_i)\Delta\omega. \tag{31}$$

To obtain the off-diagonal components of the quantum metric tensor, we can measure the excitation rate by applying the shaking along different directions. Taking g_{yz} as an example, the shaking can be applied along the directions $\hat{y} \pm \hat{z}$ [12], and then the total Hamiltonian can be written as

$$\hat{H}_{\hat{y}\pm\hat{z}}(t) = \mathcal{H}_1 + 2E(\hat{y} \pm \hat{z})\cos(\omega t), \tag{32}$$

from which we can obtain the excitation rates $\Gamma^{\text{int}}_{\hat{y}\pm\hat{z}}$, and the difference of those two excitation rates is related to the off-diagonal quantum matric tensor as

$$\Gamma^{\text{int}}_{\hat{y}+\hat{z}} - \Gamma^{\text{int}}_{\hat{y}-\hat{z}} = \frac{8\pi E^2}{\hbar^2} g_{yz}. \tag{33}$$

By shaking the optical lattice, the topological properties of tensor monopoles can be derived through the measurement of the quantum metric tensor. For our 4D system, the generalized Berry curvature $\mathcal{H}_{\mu\nu\lambda} = 4\epsilon_{\mu\nu\lambda}\sqrt{\det g_{\mu\nu}}$ can be obtained through extracting the quantum metric tensor, with which the topological charge can be obtained consequently.

Similarly, one can extract the nonzero component of Berry curvature by simply changing the time modulation as a circular time-periodic perturbation in Eq. (32), e.g.,

$$\hat{H}_{\pm}(t) = \mathcal{H}_1 + 2E[\cos(\omega t)\hat{y} \pm \sin(\omega t)\hat{z}]. \tag{34}$$

The corresponding excitation rate derived in Ref. [32] takes the following form:

$$\Gamma_{\pm}(\mathbf{k};\omega) = \frac{2\pi}{\hbar}\sum_{n=0,+} |\mathcal{V}^{\pm}_{n-}(\mathbf{k})|^2\delta^{(t)}[E_n(\mathbf{k}) - E_-(\mathbf{k}) - \hbar\omega],$$
$$|\mathcal{V}^{\pm}_{n-}(\mathbf{k})|^2 = \left(\frac{E}{\hbar\omega}\right)^2 \left|\left\langle u_n(\mathbf{k})\right| \frac{1}{i}\frac{\partial\mathcal{H}_1}{\partial k_y} \mp \frac{\partial\mathcal{H}_1}{\partial k_z}\left|u_-(\mathbf{k})\right\rangle\right|^2, \tag{35}$$

and $\delta^{(t)}(\varepsilon) = (2\hbar/\pi t)\sin^2(\varepsilon t/2\hbar)/\varepsilon^2 \to \delta(\varepsilon)$ in the long-time limit. We integrate the excitation rate $\Gamma_{\pm}(\mathbf{k}, \omega)$ over all drive frequencies $\omega \geqslant \Delta_{\text{gap}}/\hbar$ (Δ_{gap} denotes the band gap) and consider the difference between these integrated rates, which reads

$$\begin{aligned}\Delta\Gamma^{\text{int}}(\mathbf{k}) &= 4\pi\left(\frac{E}{\hbar}\right)^2 \text{Im}\sum_{n=0,+} \frac{\langle u_-|\partial_{k_y}\mathcal{H}_1|u_n\rangle\langle u_n|\partial_{k_z}\mathcal{H}_1|u_-\rangle}{(E_- - E_n)^2} \\ &= -2\pi\left(\frac{E}{\hbar}\right)^2 \Omega_{k_y,k_z},\end{aligned} \tag{36}$$

where Ω_{k_y,k_z} is one of the components of Berry curvature. This equation gives a feasible approach to measure Ω_{k_y,k_z}, and other components can also be extracted with similar methods. With the result of the Berry curvature, one could numerically obtain the longitudinal conductivity σ_{zz} from Eq. (23).

VI. CONCLUSION

In summary, we have proposed two minimal Hamiltonians which host tensor monopoles with topological charges equal to n, and we have discussed their topological properties. The topological properties and the phase transitions of the tensor monopoles with $n = 1, 2$ have been considered. By increasing h from zero, the tensor monopoles can be annihilated in pairs of opposite topological charges to open a gap. As $h > 4$, all tensor monopoles disappear and the system becomes a trivial insulator. The semiclassical Boltzmann equation has been used to calculate the longitudinal conductivity with the magnetic field; a $-B^2$ dependence of MR is obtained as a result of the Weyl semimetal with a hyperplane cutting through the two tensor monopoles. An experimental scheme of the topological charge 1 has been proposed. We suggest simulating the 4D Hamiltonian of the tensor monopole by a 3D optical lattice with a parametrized pseudomomentum along the fourth dimension. The relation between the total excitation rate and the quantum metric tensor facilitates our measurement of the quantum metric tensor by shaking the optical lattice.

ACKNOWLEDGMENTS

We thank G. Palumbo, N. Goldman, D. W. Zhang, and S. L. Zhu for helpful discussions. This work was supported by the National Key Research and Development Program of China (Grant No. 2016YFA0301800), the National Nature Science Foundation of China (Grants No. 11704180 and No. 11474153), the Key Project of Science and Technology of Guangzhou (Grant No. 201804020055) and the Key R&D Program of Guangdong Province (Grant No. 2019B030330001).

APPENDIX: CALCULATION OF THE SURFACE STATE SPECTRUM

Expanding the Hamiltonian $\mathcal{H}_2$ around $(k_x, k_y, k_z) = (0, 0, 0)$, and considering the open boundary condition along the z direction, the Hamiltonian can be rewritten as

$$\mathcal{H} = \begin{pmatrix} 0 & \hat{d}_1 - i\hat{d}_2 & 0 \\ \hat{d}_1 + i\hat{d}_2 & 0 & \hat{d}_3 + iA_{000} \\ 0 & \hat{d}_3 - iA_{000} & 0 \end{pmatrix}, \tag{A1}$$

where

$$\begin{aligned} \hat{d}_1 &= 2t\left(k_x^2 - k_y^2\right), \\ \hat{d}_2 &= 4tk_xk_y, \\ \hat{d}_3 &= 2tk_z = -2it\partial_z, \\ A_{000} &= 2t(h - 3 - \cos k_w). \end{aligned} \tag{A2}$$

We define $A_{000} \equiv \hat{d}_4$, and we regard A_{000} as a domain wall configuration along the z direction, which we choose to parametrize as

$$A_{000}(z) = \bar{A}_{000}[\Theta(z) - \Theta(-z)], \tag{A3}$$

Here $\bar{A}_{000} = -A_{000}$, and Θ is the Heaviside function with

$$\Theta(z) = \begin{cases} 1, & z > 0, \\ \frac{1}{2}, & z = 0, \\ 0, & z < 0. \end{cases} \tag{A4}$$

Since k_x and k_y are good quantum numbers, we can use their eigenvalues to replace the momentum operators and solve the eigen-equation

$$\mathcal{H}\psi = \varepsilon_k\psi, \tag{A5}$$

with $\psi = e^{ik_xx+ik_yy}\phi(z)$. The components of the spinor wavefunction $\phi(z) = (f(z), g(z), h(z))^\top$. Combining the above equations, we derive

$$\begin{aligned} f(z) &= \frac{1}{\varepsilon_k}(\hat{d}_1 - i\hat{d}_2)g(z), \\ h(z) &= \frac{1}{\varepsilon_k}(-2i\partial_z - iA_{000})g(z), \end{aligned} \tag{A6}$$

and

$$\left[-4\partial_z^2 + A_{000}^2 - 4\bar{A}_{000}\delta(z)\right]g(z) = \left[\varepsilon_k^2 - \left(\hat{d}_1^2 + \hat{d}_2^2\right)\right]g(z), \tag{A7}$$

at $z \neq 0$. The solution of Eq. (A7) is

$$h(z) = h_0e^{-|z|/\lambda}, \tag{A8}$$

where h_0 is a normalization constant and $\lambda^{-1} := \sqrt{\bar{A}_{000}^2 + (\hat{d}_1^2 + \hat{d}_2^2) - \varepsilon_\kappa^2} > 0$; the discontinuity of the delta function at $z = 0$ imposes the condition $\lambda^{-1} = \bar{A}_{000}$. Therefore, the surface states' dispersions are given by

$$\varepsilon_{\pm,k} = \pm\sqrt{\left(\hat{d}_1^2 + \hat{d}_2^2\right)} = \pm v\left(k_x^2 + k_y^2\right), \tag{A9}$$

where $v = 2t$ is the effective Fermi velocity. For $\bar{A}_{000} > 0$, we only consider $h = 3$ in the main text, so we derive $k_w \in (-\pi/2, \pi/2)$. The surface state spectrum of $\mathcal{H}_1$ can be derived with the same method.

[1] P. A. M. Dirac, Quantised singularities in the electromagnetic field, Proc. R. Soc. London Ser. A **133**, 60 (1931).

[2] H. B. Nielsen and M. Ninomiya, Absence of neutrinos on a lattice: (I). Proof by homotopy theory, Nucl. Phys. B **185**, 20 (1981).

[3] A. A. Burkov, Negative longitudinal magnetoresistance in Dirac and Weyl metals, Phys. Rev. B **91**, 245157 (2015).

[4] H.-Z. Lu and S.-Q. Shen, Quantum transport in topological semimetals under magnetic fields, Front. Phys. **12**, 127201 (2017).

[5] H.-P. Sun and H.-Z. Lu, Quantum transport in topological semimetals under magnetic fields (II), Front. Phys. **14**, 33405 (2019).

[6] D. T. Son and B. Z. Spivak, Chiral anomaly and classical negative magnetoresistance of Weyl metals, Phys. Rev. B **88**, 104412 (2013).

[7] D. W. Zhang, Y. X. Zhao, R. B. Liu, Z. Y. Xue, S. L. Zhu, and Z. D. Wang, Quantum simulation of exotic $\mathcal{PT}$-invariant topological nodal loop bands with ultracold atoms in an optical lattice, Phys. Rev. A **93**, 043617 (2016).

[8] X. Zhang, Q. Xue, and D. Zhu, Positive and negative linear magnetoresistance of graphite, Phys. Lett. A **320**, 471 (2004).

[9] X. Wan, A. M. Turner, A. Vishwanath, and S. Y. Savrasov, Topological semimetal and Fermi-arc surface states in the electronic structure of pyrochlore iridates, Phys. Rev. B **83**, 205101 (2011).

[10] G. Palumbo and N. Goldman, Revealing Tensor Monopoles through Quantum-Metric Measurements, Phys. Rev. Lett. **121**, 170401 (2018).

[11] X. Tan, D.-W. Zhang, Z. Yang, J. Chu, Y.-Q. Zhu, D. Li, X. Yang, S. Song, Z. Han, Z. Li *et al.*, Experimental Measurement of the Quantum Metric Tensor and Related Topological Phase Transition with a Superconducting Qubit, Phys. Rev. Lett. **122**, 210401 (2019).

[12] T. Ozawa and N. Goldman, Extracting the quantum metric tensor through periodic driving, Phys. Rev. B **97**, 201117(R) (2018).

[13] M. Yu, P. Yang, M. Gong, Q. Cao, Q. Lu, H. Liu, S. Zhang, M. B. Plenio, F. Jelezko, T. Ozawa *et al.*, Experimental measurement of the quantum geometric tensor using coupled qubits in diamond, Natl. Sci. Rev. **7**, 254 (2020).

[14] A. Gianfrate, O. Bleu, L. Dominici, V. Ardizzone, M. De Giorgi, D. Ballarini, G. Lerario, K. W. West, L. N. Pfeiffer, D. D. Solnyshkov *et al.*, Measurement of the quantum geometric tensor and of the anomalous Hall drift, Nature (London) **578**, 381 (2020).

[15] X. Tan, D.-W. Zhang, D. Li, X. Yang, S. Song, Z. Han, Y. Dong, D. Lan, H. Yan, S.-L. Zhu, and Y. Yu, Experimental

observation of tensor monopoles with a superconducting qudit, arXiv:2006.11770.
[16] M. Chen, C. Li, G. Palumbo, Y.-Q. Zhu, N. Goldman, and P. Cappellaro, Experimental characterization of the 4D tensor monopole and topological nodal rings, arXiv:2008.00596.
[17] D.-W. Zhang, Y.-Q. Zhu, Y. X. Zhao, H. Yan, and S.-L. Zhu, Topological quantum matter with cold atoms, Adv. Phys. **67**, 253 (2018).
[18] H. M. Price, O. Zilberberg, T. Ozawa, I. Carusotto, and N. Goldman, Four-Dimensional Quantum Hall Effect with Ultracold Atoms, Phys. Rev. Lett. **115**, 195303 (2015).
[19] M. Lohse, C. Schweizer, H. M. Price, O. Zilberberg, and I. Bloch, Exploring 4D quantum Hall physics with a 2D topological charge pump, Nature (London) **553**, 55 (2018).
[20] O. Boada, A. Celi, J. I. Latorre, and M. Lewenstein, Quantum Simulation of an Extra Dimension, Phys. Rev. Lett. **108**, 133001 (2012).
[21] A. Celi, P. Massignan, J. Ruseckas, N. Goldman, I. B. Spielman, G. Juzeliūnas, and M. Lewenstein, Synthetic Gauge Fields in Synthetic Dimensions, Phys. Rev. Lett. **112**, 043001 (2014).
[22] S.-L. Zhu, Z.-D. Wang, Y.-H. Chan, and L.-M. Duan, Topological Bose-Mott Insulators in a One-Dimensional Optical Superlattice, Phys. Rev. Lett. **110**, 075303 (2013).
[23] S. Ganeshan and S. Das Sarma, Constructing a Weyl semimetal by stacking one-dimensional topological phases, Phys. Rev. B **91**, 125438 (2015).
[24] O. Zilberberg, S. Huang, J. Guglielmon, M. Wang, K. P. Chen, Y. E. Kraus, and M. C. Rechtsman, Photonic topological boundary pumping as a probe of 4D quantum Hall physics, Nature (London) **553**, 59 (2018).
[25] F. Mei, S. L. Zhu, Z. M. Zhang, C. H. Oh, and N. Goldman, Simulating Z_2 topological insulators with cold atoms in a one-dimensional optical lattice, Phys. Rev. A **85**, 013638 (2012).
[26] Y. L. Chen, G. Q. Zhang, D. W. Zhang, and S. L. Zhu, Simulating bosonic Chern insulators in one-dimensional optical superlattices, Phys. Rev. A **101**, 013627 (2020).
[27] D.-W. Zhang, L.-Z. Tang, L.-J. Lang, H. Yan, and S.-L. Zhu, Non-Hermitian topological Anderson insulators, Sci. China Phys., Mech. Astron. **63**, 267062 (2020).
[28] N. Fläschner, B. S. Rem, M. Tarnowski, D. Vogel, D.-S. Lhmann, K. Sengstock, and C. Weitenberg, Experimental reconstruction of the Berry curvature in a Floquet Bloch band, Science **352**, 1091 (2016).
[29] T. Li, L. Duca, M. Reitter, F. Grusdt, E. Demler, M. Endres, M. Schleier-Smith, I. Bloch, and U. Schneider, Bloch state tomography using Wilson lines, Science **352**, 1094 (2016).
[30] L. Duca, T. Li, M. Reitter, I. Bloch, M. Schleier-Smith, and U. Schneider, An Aharonov-Bohm interferometer for determining Bloch band topology, Science **347**, 288 (2015).
[31] M. Wimmer, H. M. Price, I. Carusotto, and U. Peschel, Experimental measurement of the Berry curvature from anomalous transport, Nat. Phys. **13**, 545 (2017).
[32] D. T. Tran, A. Dauphin, A. G. Grushin, P. Zoller, and N. Goldman, Probing topology by "heating": Quantized circular dichroism in ultracold atoms, Sci. Adv. **3**, e1701207 (2017).
[33] R. I. Nepomechie, Magnetic monopoles from antisymmetric tensor gauge fields, Phys. Rev. D **31**, 1921 (1985).
[34] C. Teitelboim, Monopoles of higher rank, Phys. Lett. B **167**, 69 (1986).
[35] P. Orland, Instantons and disorder in antisymmetric tensor gauge fields, Nucl. Phys. B **205**, 107 (1982).
[36] M. Kalb and P. Ramond, Classical direct interstring action, Phys. Rev. D **9**, 2273 (1974).
[37] C. Fang, M. J. Gilbert, X. Dai, and B. A. Bernevig, Multi-Weyl Topological Semimetals Stabilized by Point Group Symmetry, Phys. Rev. Lett. **108**, 266802 (2012).
[38] M. Gell-Mann, in *Murray Gell-Mann: Selected Papers* (World Scientific, Singapore, 2010), pp. 128–145.
[39] Y.-Q. Zhu, N. Goldman, and G. Palumbo, Four-dimensional semimetals with tensor monopoles: From surface states to topological responses, Phys. Rev. B **102**, 081109(R) (2020).
[40] V. Mathai and G. C. Thiang, Differential topology of semimetals, Commun. Math. Phys. **355**, 561 (2017).
[41] M. K. Murray, Bundle gerbes, J. London Math. Soc. **54**, 403 (1996).
[42] N. J. Hitchin, *The Many Facets of Geometry: A Tribute to Nigel Hitchin* (Oxford University Press, Oxford, 2010).
[43] V. Cortés, *Handbook of Pseudo-Riemannian Geometry and Supersymmetry*, IRMA Lectures in Mathematics and Theoretical Physics Vol. 16 (European Mathematical Society, Berlin, 2010).
[44] J. Provost and G. Vallee, Riemannian structure on manifolds of quantum states, Commun. Math. Phys. **76**, 289 (1980).
[45] T. Neupert, L. Santos, S. Ryu, C. Chamon, and C. Mudry, Noncommutative geometry for three-dimensional topological insulators, Phys. Rev. B **86**, 035125 (2012).
[46] G. Palumbo and N. Goldman, Tensor Berry connections and their topological invariants, Phys. Rev. B **99**, 045154 (2019).
[47] S.-T. Wang, D.-L. Deng, and L.-M. Duan, Probe of Three-Dimensional Chiral Topological Insulators in an Optical Lattice, Phys. Rev. Lett. **113**, 033002 (2014).
[48] D.-L. Deng, S.-T. Wang, and L.-M. Duan, Direct probe of topological order for cold atoms, Phys. Rev. A **90**, 041601(R) (2014).
[49] D. Culcer, Transport in three-dimensional topological insulators: Theory and experiment, Physica E **44**, 860 (2012).
[50] X. Dai, Z. Z. Du, and H.-Z. Lu, Negative Magnetoresistance without Chiral Anomaly in Topological Insulators, Phys. Rev. Lett. **119**, 166601 (2017).
[51] G. Sundaram and Q. Niu, Wave-packet dynamics in slowly perturbed crystals: Gradient corrections and Berry-phase effects, Phys. Rev. B **59**, 14915 (1999).
[52] D. Xiao, M.-C. Chang, and Q. Niu, Berry phase effects on electronic properties, Rev. Mod. Phys. **82**, 1959 (2010).
[53] R. Shindou and K.-I. Imura, Noncommutative geometry and non-Abelian Berry phase in the wave-packet dynamics of Bloch electrons, Nucl. Phys. B **720**, 399 (2005).
[54] D. Xiao, W. Yao, and Q. Niu, Valley-Contrasting Physics in Graphene: Magnetic Moment and Topological Transport, Phys. Rev. Lett. **99**, 236809 (2007).
[55] A. A. Burkov, Chiral Anomaly and Diffusive Magnetotransport in Weyl Metals, Phys. Rev. Lett. **113**, 247203 (2014).
[56] H. M. Price and N. R. Cooper, Mapping the Berry curvature from semiclassical dynamics in optical lattices, Phys. Rev. A **85**, 033620 (2012).
[57] Y. Q. Zhu, D. W. Zhang, H. Yan, D. Y. Xing, and S. L. Zhu, Emergent pseudospin-1 Maxwell fermions with a threefold degeneracy in optical lattices, Phys. Rev. A **96**, 033634 (2017).

[58] S.-L. Zhu, B. Wang, and L.-M. Duan, Simulation and Detection of Dirac Fermions with Cold Atoms in an Optical Lattice, Phys. Rev. Lett. **98**, 260402 (2007).

[59] D.-W. Zhang, S.-L. Zhu, and Z. D. Wang, Simulating and exploring Weyl semimetal physics with cold atoms in a two-dimensional optical lattice, Phys. Rev. A **92**, 013632 (2015).

[60] M. Kolodrubetz, D. Sels, P. Mehta, and A. Polkovnikov, Geometry and non-adiabatic response in quantum and classical systems, Phys. Rep. **697**, 1 (2017).

[61] M. Aidelsburger, S. Nascimbene, and N. Goldman, Artificial gauge fields in materials and engineered systems, C. R. Phys. **19**, 394 (2018).

[62] L. Lu, J. D. Joannopoulos, and M. Soljačić, Topological photonics, Nat. Photonics **8**, 821 (2014).

[63] A. Eckardt, Colloquium: Atomic quantum gases in periodically driven optical lattices, Rev. Mod. Phys. **89**, 011004 (2017).

[64] D. W. Zhang, F. Mei, Z. Y. Xue, S. L. Zhu, and Z. D. Wang, Simulation and measurement of the fractional particle number in one-dimensional optical lattices, Phys. Rev. A **92**, 013612 (2015).

[65] M. Reitter, J. Nager, K. Wintersperger, C. Strater, I. Bloch, A. Eckardt, and U. Schneider, Interaction Dependent Heating and Atom Loss in a Periodically Driven Optical Lattice, Phys. Rev. Lett. **119**, 200402 (2017).

[66] N. Flaschner, M. Tarnowski, B.S. Rem, D. Vogel, K. Sengstock, and C. Weitenberg, High-precision multiband spectroscopy of ultracold fermions in a nonseparable optical lattice, Phys. Rev. A **97**, 051601(R) (2018).

[67] M. Aidelsburger, M. Lohse, C. Schweizer, M. Atala, J. T. Barreiro, S. Nascimbne, N. R. Cooper, I. Bloch, and N. Goldman, Measuring the Chern number of Hofstadter bands with ultracold bosonic atoms, Nat. Phys. **11**, 162 (2015).

[68] F. Mei, J. B. You, D. W. Zhang, X. C. Yang, R. Fazio, S. L. Zhu, and L. C. Kwek, Topological insulator and particle pumping in a one-dimensional shaken optical lattice, Phys. Rev. A **90**, 063638 (2014).

[69] G. Liu, S. L. Zhu, S. Jiang, F. Sun, and W. M. Liu, Simulating and detecting the quantum spin Hall effect in the kagome optical lattice, Phys. Rev. A **82**, 053605 (2010).

[70] S.-L. Zhu, H. Fu, C.-J. Wu, S.-C. Zhang, and L.-M. Duan, Spin Hall Effects for Cold Atoms in a Light-Induced Gauge Potential, Phys. Rev. Lett. **97**, 240401 (2006).

[71] I. Souza, T. Wilkens, and R. M. Martin, Polarization and localization in insulators: Generating function approach, Phys. Rev. B **62**, 1666 (2000).

[72] R. Resta, The insulating state of matter: A geometrical theory, Eur. Phys. J. B **79**, 121 (2011).

[73] I. Souza and D. Vanderbilt, Dichroic f-sum rule and the orbital magnetization of crystals, Phys. Rev. B **77**, 054438 (2008).

[74] F. de Juan, A. G. Grushin, T. Morimoto, and J. E. Moore, Quantized circular photogalvanic effect in Weyl semimetals, Nat. Commun. **8**, 15995 (2017).

[75] D. T. Tran, N. R. Cooper, and N. Goldman, Quantized Rabi oscillations and circular dichroism in quantum Hall systems, Phys. Rev. A **97**, 061602(R) (2018).

[76] M. Schüler and P. Werner, Tracing the nonequilibrium topological state of Chern insulators, Phys. Rev. B **96**, 155122 (2017).